Decay processes in buildings close to the sea induced by marine aerosol: Salt depositions inside construction materials

H. Morillas, F.F. Mendonça Filho, Hannelore Derluyn, M. Maguregui, David Grégoire, Juan Manuel Madariaga

*Graphical Abstract

HIGHLIGHTS

- Nature and distribution of salts crystallizations in building materials of a construction close to the sea has been studied.
- XRD and Raman microscopy allowed to define the wide variety of sulfates presence.
- To define the chlorine presence EDXRF imaging should be implemented in the methodology.
- In some of the building materials both sulfates and chlorides concentration are close to 3% w/w.

Decay processes in buildings close to the sea induced by marine aerosol: Salt depositions inside construction materials

Héctor Morillas[1, 2], Fernando França de Mendonça Filho[3]*, Hannelore Derluyn[3], Maite Maguregui[4], David Gregoire[3, 5], Juan Manuel Madariaga[1]

[1]Department of Analytical Chemistry, Faculty of Science and Technology, University of the Basque Country UPV/EHU, P.O. Box 644, 48080 Bilbao, Basque Country, Spain
[2]Department of Mathematics and Experimental Sciences Didactics, Faculty of Education, Philosophy and Anthropology, University of the Basque Country UPV/EHU, II Building, Oñati Plaza 3, 20018 Donostia-San Sebastian, Basque Country, Spain e-mail: hector.morillas@ehu.es
[3]Universite de Pau et des Pays de l'Adour, E2S UPPA, CNRS, Total, LFCR, Anglet-Pau, France
[4]Department of Analytical Chemistry, Faculty of Pharmacy, University of the Basque Country UPV/EHU, P.O. Box 450, 01080 Vitoria-Gasteiz, Basque Country, Spain
[5]Institut Universitaire de France
* currently at: Department of Materials, Mechanics, Management and Design, Faculty of Civil Engineering and Geosciences, Delft University of Technology, P.O. Box 5048, 2600 GA, Delft, Netherlands

Abstract

Buildings close to the sea experience different kinds of decay processes related with the influence of marine aerosol. This sea spray is a chemically complex system formed by inorganic salts (sulfates, nitrates and mainly chlorides) and organic matter, together even with airborne particulate matter from the surrounding environment. Buildings close to the sea, erected using different materials such as bricks, plasters, limestones and sandstones, can experience many kinds of chemical reactions promoted by the impact of this sea spray, which favour the formation of salt crystallizations. In this work, a study of salts crystallizing in different kinds of building materials of a construction close to the Bay of Biscay (Villa Belza, Biarritz, France) has been studied in order to evaluate the state of conservation of the materials under study. The construction materials affected by salts were analysed by means of X-ray Diffraction (XRD) and μ-Raman spectroscopy (μ-RS) for molecular analyses, Energy dispersive X-ray Fluorescence spectrometry (μ-ED-XRF) for elemental analyses and soluble salts tests by means of ion chromatography. These analyses revealed different levels of chlorides, nitrates and sulfates. Moreover, using this methodology, some specific chemical reactions that take place in the Villa Belza were understood. This knowledge can help to lay the foundations for possible future restoration works.

Keywords: marine aerosol, limestone, sandstone, XRD, ED-XRF, Ion Chromatography.

1. Introduction

Buildings erected close to the sea can experience more chemical decay processes than others. These decay processes are usually alterations derived from physical or chemical interaction between building materials and the surrounding environment. This negative influence is closely related with marine aerosol. Marine aerosol is a chemical complex system formed by inorganic salts **(Morillas et al. 2016a; 2018a)** and organic matter **(Bao et al., 2018; Miyazaki et al., 2018)**, together with airborne particulate matter **(Calparsoro et al., 2017)**. The primary particles transported in the marine aerosol (PMA) can induce different chemical reactions in the atmosphere **(Ceburnis et al., 2016**; **Xiao et al., 2018)**, promoting the so-called Secondary Marine Aerosol (SMA) particles **(O'Dowd and de Leeuw, 2007)**. These kinds of particles, together with the natural crustal or mineral particles and the metallic airborne particulate matter emitted by anthropogenic sources (road traffic, industry, etc.) can be deposited on building materials from a specific construction following dry deposition processes **(Morillas et al., 2016a)**. The interactions of these natural and anthropogenic stressors with building materials can promote different kinds of pathologies.

One of the most aggressive deterioration pathways promoted by marine aerosol is salt crystallization **(Vallet et al., 2006)** and thus the presence of soluble salts in the building materials used to erect construction. The damages caused by soluble salts in the building materials can be produced as result by several mechanisms based on the kind of crystallization **(Granneman et al., 2019; Derluyn et al., 2014; Celik and Aygun, 2018)**.

The formation of these salts is not only an aesthetical problem when they become visible as efflorescences **(Kamh et al., 2017)**. The main problem resides when salts precipitate beneath the material as subflorescences **(Morillas et al., 2015)**. Indeed, its formation during time can get to crack materials and cause irreparable loss of material in the building. In this way, the level of damage by marine aerosol can vary depending on the characteristics of the material, such as limestone **(Derluyn et al., 2013; 2019)**, sandstone **(Raneri et al., 2015)**, bricks **(Morillas et al., 2018b)** and plaster **(Morillas et al., 2013)**.

The crystallization process occurs when the salt solubility is being exceeded, the salt solubility itself being temperature dependent **(Onasch et al., 2000; Gomez-Heras and Fort, 2007; Zhang et al., 2014)**. When occurring in a building material, the pore size **(Cultrone and Sebastian, 2008)**, water absorption capacity **(Yang and Wang, 2019)**, mechanical strength **(Chunran and Shicong, 2019)** and pore size distribution **(Molina et al., 2011)** of the material play their role as well in salt-induced decay. The deposition and the crystal solubilization, and subsequently the entry of these soluble salts into the building material promotes the crystal growing in pores, or subsequent crystallizations in existing fissures, which gives rise to tensions promoting the enlargement of these areas **(Ruedrich et al., 2007; Thiebaut et al., 2018)**. Under confined conditions, i.e. within the pores of the building material or within an existing fissure, the crystallization exerts a certain stress on the pore or fissure wall **(Espinosa et al., 2008a)**, proportional to the natural logarithm of the supersaturation degree **(Espinosa et al., 2008b)**. If this physical stress exceeds the tensile strength of the material, deterioration occurs.

For all these reasons, analytical monitoring of building materials as well as conservation interventions are strongly recommended in any process of decision-making related to the soluble salts presence **(Mendonça Filho et al., 2019; Morillas et al., 2016b)**, with crystallization-induced decay one of the most aggressive deterioration processes affecting buildings erected in coastal areas.

In this work, a multianalytical methodology based on the combination of X-ray Diffraction (XRD) and μ-Raman spectroscopy (μ-RS) for molecular analyses, Energy dispersive X-ray Fluorescence spectrometry (ED-XRF) for elemental analyses and soluble salts tests by means of ion chromatography was applied to the characterization of building materials used for the construction of the Villa Belza (Biarritz, France) and affected by the action of marine aerosol action.

2. Materials and methods

2.1. Location and Sampling

This study has been carried out on the façades from a building called the Villa Belza, which was built from 1880 until 1895. The construction is located at the coast of Biarritz, France, with direct exposition to sea spray (see Figure S1 from Supplementary Material and Table 1). The study has been performed in the façade opposite to the

orientation of the sea, since it was not possible to extract samples from the opposite façade oriented directly to the sea. 23 samples of different kinds of materials (limestones, sandstone, cement and joint and rendering mortars) were collected at different heights (see Figure 1) in order to observe possible differences in the deterioration processes of building materials along the façade.

2.2. Instrumentation

For the molecular characterization of the 23 samples analyzed, XRD analyses were carried out using a powder diffractometer PANalytical Xpert PRO instrument equipped with a copper tube (λCuKα1= 1.54060 Å, λCuKα2= 1.54439 Å), a vertical goniometer (Bragg-Brentano geometry), a programmable divergence aperture, an automatic interchange of samples, a secondary monochromator of graphite and a PixCel detector. The measurement conditions were 40 kV and 40 mA, with an angular range (2θ) scanned between 5 and 70°. Moreover, X`pert HighScore (PANalytical) software in combination with the specific powder diffraction file database (International Centre for Diffraction Data - ICDD, Pennsylvania, USA) was used for the data treatment of the diffractograms and the identification of the present mineral phases.

In order to obtain complementary molecular information present in the Villa Belza samples, Raman spectroscopy was used. For the micro-Raman analyses, the inVia Renishaw confocal Raman microspectrometer (Renishaw, Gloucestershire, UK) coupled to a DMLM Leica microscope with 5×, 20× and 50× long working distance lens was used. A 514 nm excitation laser (with nominal laser power at 50 mW) was used. The spectrometer was daily calibrated by using the 520.5 cm^{-1} Raman band of a silicon chip. Lasers were set at low power (not more than 1 mW at the sample) to avoid sample decomposition. Data acquisition was carried out using the Wire 4.2 software package (Renishaw). Spectra were acquired in the spectral region between 100 and 3000 cm^{-1}. Measurements were acquired between 5-30 s and several scans (between 10-40 scans) were accumulated for each spectrum to improve the signal-to-noise ratio. To interpret all the Raman results, the acquired Raman spectra were compared with Raman spectra of pure standard compounds collected in the e-VISNICH dispersive Raman database **(Maguregui et al., 2010)** and with free Raman databases (e.g. RRUFF **(Downs and Hall-Wallace, 2002)**) for the assignation of Raman bands. For the spectral treatment and analysis, Wire 2.0 (Renishaw, Gloucestershire, UK) and OMNIC® 7.2

138 software (Thermo Nicolet, Madison, WI, USA) were used. Once the compounds were
139 identified, they were classified as original or deterioration compounds. A given
140 compound is said to be identified if it appeared at least five times in different spectra
141 from the same sample.

142 For the elemental analysis of the samples, the M4 TORNADO (Bruker Nano GmbH,
143 Berlin, Germany) energy dispersive X-Ray fluorescence spectrometer (EDXRF) was
144 used. Measurements were conducted directly in the rock fragments using poly-capillary
145 lens, which are able to achieve a lateral resolution down to 25 μm (measured at the Mo
146 Kα line). The X-ray Rh anode tube implemented operates at up to 50 kV with a
147 maximum current of 600 μA, which were the conditions considered for the spectral
148 acquisition. The detection of the fluorescence radiation was performed by an XFlash®
149 silicon drift detector with 30 mm^2 sensitive area and energy resolution of 145eV for
150 Mn-Kα. In order to improve the detection of the lightest elements ($Z<19$), filters were
151 not used and measurements were acquired under vacuum (20 mbar). To achieve the
152 vacuum, a diaphragm pump MV 10 N VARIO-B (Vaccubrand, Wertheim, Germany)
153 was used. The live time used for each punctual measurement was 200 seconds. The
154 spectral data acquisition and treatment was performed using the M4 TORNADO
155 software (Bruker Nano GmbH, Berlin, Germany).

156 To determine the nature of the main colonizers in the greenish patina visible in some
157 samples (e.g., S8 sample in Figure 1) from Villa Belza, Phase Contrast microscope
158 (PCM) was used. Micro-photographs of the colonized samples were obtained with a
159 Nikon DN100 camera coupled to a Nikon SMZ800 stereoscopic microscope and
160 microphotographs were captured with a Nikon DS Fi1 DS-Fi1 digital microscope
161 camera on a Nikon Eclipse 80i PCM provided with 20×, 40×, 60× and 100× objective
162 lenses.

163 The quantification of soluble salts, present in the samples of the limestone, sandstone,
164 cement and joint and rendering mortars from Villa Belza, was conducted by ion
165 chromatography with conductivity detection after post-column ion suppression. Prior to
166 the soluble salt quantification, an extraction of the soluble cations and anions was
167 carried out using an ultrasound-based extraction method. All the samples were
168 homogenized in an agate mortar and dried in an oven at 75 ºC until constant weight.
169 After that, powdered and dried samples were subjected to an ultrasound extraction

procedure in an ultrasound bath. 100 mg of powdered sample with 100 ml of Milli-Q quality water (Millipore, USA) was placed in an ultrasound bath during 100 min in order to extract soluble salts (anions and cations) from samples. Cations (Ca^{2+}, K^{+}, Na^{+}, Mg^{2+}, NH_4^{+}) and anions (Cl^{-}, NO_3^{-}, SO_4^{2-}) were quantified by means of ion chromatography. For cations a Dionex UCS-5000 ion chromatograph and for anions a Dionex ICS-2500 ion chromatograph connected to a conductimetric detector (ED50 Dionex conductimetric detector) with post-column suppression (Thermo Scientific™ Dionex CERS 500, Dionex Corporation, Sunnyvaley, California, USA) was employed. The experimental conditions used for the quantification of these anions are described elsewhere **(Prieto-Taboada et al. 2012)**.

3. Results and discussion

3.1. Molecular analyses of the construction materials

To determine the mineralogical composition of the construction materials of Villa Belza, XRD analyses were carried out. In Table 1, a summary of the semi-quantitative estimation of the minerals present in the analyzed samples in weight percentage (wt %) is presented. This estimation is based on the intensity (height) of the most intense peak or diffraction maximum of each phase, and on the RIR (Reference Intensity Ratio) value contained in the Powder Diffraction Files (PDF) referenced to the database **(Zhou et al., 2018)**. The estimation is based on a single peak for each phase, mainly free of interference with peaks of other phases. In some cases, their relative intensity might be affected in the case of phases with preferential orientation. The RIR values are fundamentally empirical and may vary somewhat between different PDF files of the same mineral. In this calculation, only the identified phases are taken into consideration for the semi-quantitative estimation, reaching the 100 %. In this sense, the unidentified phases and the amorphous (non-crystalline) material that the samples could contain are not considered. These estimations may be useful as a first approach, especially for comparison among samples.

As can be seen in the Table 1, the principal mineralogical phases present in almost all the samples were calcite ($CaCO_3$) and quartz (α-SiO_2) contributing with different percentages according to the type of material. Moreover, gypsum ($CaSO_4 \cdot 2H_2O$) and

halite (NaCl) are also present with variation in their percentages (2-7% and 1-2% respectively).

The highest content of gypsum was detected in S20 sandstone sample and samples S3, S4 and S23 (rendering mortars). In these last rendering mortars, the highest concentrations (2%) of halite (NaCl) was also detected. Both, sulfates and chlorides, are closely related with the influence of marine aerosol. On the one hand, sulfates present in the sea spray, together with the H_2CO_3 aerosol, can react with the carbonaceous materials giving rise to the subsequent calcium sulfates. In this way, calcium carbonate is a highly soluble carbonate that can be dissolved due to the action of CO_2 dissolved in atmospheric aerosols (see reaction 1) and therefore the solubilized Ca^{2+} can react with the SO_4^{2-} coming from sea spray (see reactions 2) giving rise to gypsum formation after a previous formation of anhydrite ($CaSO_4$).

$$CaCO_3\,(s) + H_2CO_3\,(dis) \leftrightarrows Ca^{2+} + 2HCO_3^- \quad \textbf{(1)}$$

$$Ca^{2+} + SO_4^{2-} \leftrightarrows CaSO_4\,(dis) \leftrightarrows CaSO_4 \cdot 2H_2O\,(s) \quad \textbf{(2)}$$

On the other hand, the halite present in the sample at concentrations between 1-2% can be present in the building materials coming from the dry deposition of marine aerosol. Chlorides can migrate to the inner areas and re-crystallize, promoting NaCl subflorescence, which under natural radiation can produce partial disruption of the porous surface, producing micro-spallings **(Gómez-Heras and Fort, 2007)**. This kind of pathology is visible in Villa Belza contruction.

In samples S4 (rendering mortar) and S15 (joint mortar) apart from the mentioned compounds, additional specific decay compounds were also detected (see Figure 2). In Figure S4, apart from calcite and quartz (matrix composition), halite and portlandite were also detected (see Figure 2A). As explained above, halite presence is related to the marine influence, but portlandite ($Ca(OH)_2$) presence cannot be connected to this stressor source. Portland cement can suffer different decay processes. The cement typically provides to a building construction an alkaline protection with a pH around 12. Nevertheless, sometimes, due to the surrounding environment, this pH can decrease to 10 losing its inherent protection. Consequence of it is the carbonation of the cement (reaction between atmospheric CO_2 and the $Ca(OH)_2$, which can be catalyzed by chlorides and sulfates from marine aerosol **(Broomfield, 2006).**

In sample S15, apart from calcite and quartz, pyroaurite ($Mg_6Fe_2(CO_3)(OH)_{16}\cdot 4H_2O$) and ettringite ($Ca_6Al_2(SO_4)_3(OH)_{12}\cdot 26H_2O$) were also detected (see Figure 2B). As it is known, for the preparation of mortars, sand, water and a binder (hydraulic and non-hydraulic lime or cement) are used. This cement is obtained by calcination of calcite and clay that later is milled producing the clinker (composed by different lime silicates) **(Elsen, 2006).** Subsequently, the cement included in the constructions can suffer the influence of marine aerosol. The material reacts with the chlorides and sulfates mainly present in the aerosol, leading to chemical reactions inside the cement pores **(García-Florentino et al., 2016)**. An example of it is the formation of ettringite **(Apostolopoulou et al., 2018)**, which can lead to expansive reactions leading to material cracking. Regarding pyroaurite ($Mg_6Fe_2(CO_3)(OH)_{16}.4H_2O$), there are works that previously described its formation in laboratory controlled conditions. For the formation of this compound, $FeCO_3$ and Mg-rich environment with oxidation processes at a pH of 8.5 is necessary **(Hansen and Taylor, 1990).**

Additionally, in sample S13 (sandstone) a greenish color was observed. In this sample, the main component was quartz (95% of α-SiO_2), calcite (2% of $CaCO_3$), gypsum (2% of $CaSO_4\cdot 2H_2O$) and halite (1% of NaCl). The XRD diffractogram of sample S13 showed an elevation of the spectral background that suggested the existence of amorphous phases (organic or non-crystalline). Considering that the greenish patina in the sample can be related with a biocolonization (see Figure S2 from Supplementary Material), the sample was investigated by means of Phase Contrast Microscopy (PCM). Thanks to the microscopic observations, many cyanobacteria colonies were identified. As it can be seen in Figure S3A and S3B from Supplementary Material, different characteristics of coccoid cells and cyanobacterial cells in division even showing their pseudo-filaments were observed. Finally, cyanobacterial cells with their endospores or baeocytes were also observed (see Figure S3C and S3D from Supplementary Material). These microscopic observations–suggest that the greenish color is connected to the cyanobacteria colonies; more specifically the *Pleurocapsales* order and the gender *Pleurocapsa*. This kind of cyanobacteria typically colonize high content quartz limestones **(Shalygin et al., 2019)**.

In the sample S20, the main mineralogical phases were quartz (80%), calcite (12%), gypsum (7%) and halite (1%). The semi-quantitative content of calcite is relatively low (12%), but taking into account the high content of gypsum (7%), it is clear that a

sulfation process is taking place in this area. The calcite present in this sandstone sample can be transformed into gypsum through a sulfation process promoted by the load of sulfates present in the marine aerosol **(Zezza and Macri, 1995)**. These reactions have been described previously (see reactions 1-2).

Additionally, Raman microscopy was performed to complement the molecular information obtained by XRD. Owing to the fact that using XRD it is not possible to determine amorphous mineral phases or minor compounds (below 1% in weight), Raman microscopy was used to complement the possible detection of additional compounds at minor or trace levels. For this reason, apart from the same mineralogical phases observed by XRD, additional ones were also detected by Raman spectroscopy. In many samples, aluminosilicates such as adularia ($KAlSi_3O_8$); quartz (SiO_2); rutile (TiO_2); calcite ($CaCO_3$) and charcoal (C) were also identified

In most of the studied samples (S1, S2, S9, S10, S11, S12, S13, S14 and S20) different kind of calcium sulfates were detected (see Figure 3), such as gypsum (main Raman bands at 414, 493, 616, 670, 1008 and 1132 cm^{-1}) (see Figure 3A), bassanite ($CaSO_4 \cdot ½H_2O$, main Raman bands at 430, 488, 627, 668 and 1015 cm^{-1}) (see Figure 3B) and anhydrite ($CaSO_4$, main Raman bands at 422, 492, 631, 673, 1024 and 1166 cm^{-1}) (see Figure 3C). In this last case, the additional band at 1086 cm^{-1} that belongs to calcite (see Figure 3C) was also registered. The identification of calcium sulfate crystallization with different hydration waters is related with the dehydration process of the gypsum previously formed in the different building materials (sandstone, limestone and joint and rendering mortar) from Villa Belza construction. These transformations start when water evaporation processes take place under some specific reactions described elsewhere **(Morillas et al., 2013).** Hydration and dehydration cycles promote an increase and decrease in the size of the crystals formed in the pores of the building materials, which can lead to possible cracks and loss of material.

3.2. Elemental analysis of the construction materials

In addition to the molecular measurements, μ-EDXRF imaging analysis was also performed to extract additional conclusions about the conservation state of the materials used in the Villa Belza construction. First, different single point EDXRF spectra (down to 25 μm of lateral resolution) were acquired to identify the elements of interest. After that, different mappings were performed. In Figure 4, an example of the elemental

distribution maps obtained in sample S15 (joint mortar) is displayed. Although some elements such as Pb, As, Fe, Co and Cu are quite homogeneously distributed in the mapped area (see Figure 4A to D), specific hotspots of these elements which show a higher intensity of their respective K_α lines (except for Pb, which L_α line was used for data interpretation) are also observable. Elements such as Ti-V-Cr (see Fig 4E) are heterogeneously distributed in the sample.

Moreover, in the whole section of the joint mortar, aluminosilicates are widely distributed (see K-Al-Si distribution in Figure 4F), probably as adularia or microcline according to XRD and Raman results. In the Figure 4G the clear distribution of the aggregate (Si) and the binder (Ca) is observable. The white central vein in the mapped area is connected not only to Ca, but also to Mg (see Figure 4F and H), which can suggest a mixed presence of calcite and dolomite, the presence of Mg-rich calcite or even dolomite ($CaMg(CO_3)_2$). This last carbonate was identified in some of the samples considered in this work (see Table 1). The non-detection of it in sample S15 does not imply that this carbonate is not present, because it can be set under the detection limit of the applied XRD methodology.

It is also remarkable that in samples S15, Zn is specifically accumulated in a concrete position in the mapped area (see Figure 4F). In some areas of the analyzed sample, the distribution of Ca and S is coincident (see pink-purple areas in Figure 4H), suggesting the possible presence of calcium sulfates (gypsum, anhydrite or basanite) in the inner part of the joint mortar. Calcium sulfates were not identified in this sample by XRD probably because their concentration was set under the limit of detection of the technique. In this sense, if an elemental study had not been accomplished, the identification of sulfates at low concentrations in the sample would not have been carried out.

Apart from sulfates, the high correlation between Na and Cl distribution maps (see Figure 4I) suggests the crystallization of NaCl inside the S15 joint mortar. Once more, this halide was not detected by XRD. Halite crystallizations can promote many physical problems in the building material structures promoting cracks and loss of material. Additionally, Cl-Mg showed coincident distributions (greenish yellow in the Figure 4J) in the corners of the central vein, both elements present in the marine aerosol.

Different elemental mappings obtained from S17 and S7 samples respectively are also presented in the Figures S4 and S5 from the Supplementary Material. Regarding the original components in the samples (calcite and aluminosilicates mainly), the conclusions that can be extracted are quite similar to those obtained for sample S15.

On the one hand, in sample S17, the areas showing a coincident distribution of Ca and S (see Figure S4 from Supplementary Material) are lower than the ones detected in S15, which suggest a lower presence of calcium sulfates. Once again, the white vein detected in this sample also shows a high correlation between Ca and Mg, being possible to extract the same conclusion previously introduced. In this sample, it is clearly evident that NaCl is widely distributed (see Figure S4 from Supplementary Material), suggesting a high impact of marine aerosol in the mentioned sample. On the other hand, sample S7 belongs to a section of a limestone from the construction. In it, the punctual presence of silicates and some aluminosilicates are also observable (see Figure S5 from Supplementary Material). In some specific areas where aluminosilicates are present, the intensity of the Fe, Ti, V and Cr K_α line is also higher, suggesting a possible contribution of these metals in the aluminosilicates. In this sample also, although the intensity of the Ca line is much higher than the one of S, both elements showed a coincident distribution (purple areas in Figure S5 from Supplementary Material), which suggest a possible sulfation of the limestome. In this case, also, the presence of NaCl crystallizations are also visible due to the coincident distribution of Na and Cl (see Figure S5 from Supplementary Material). As in the previous samples, in this case also it was not possible to detect the presence of calcium sulfates and halite in the XRD diffractograms, suggesting that both kind of salts crystallizations could be set at concentrations lower than 1 %. Additionally, many different potassium and iron alumino silicates, mica ($AC_{2\text{-}3}T_4O_{10}X_2$) and possible kaolinite ($Al_2Si_2O_5(OH)_4$) were also observed in S7 as component of the limestones used for Villa Belza construction (see Figure S5 from Supplementary Material). Moreover, others elements such as Co and Mn-Fe are also quite homogeneous distributed and elements such as Ti-Cr-V, heterogeneous distributed in the limestone matrix.

3.3. Quantification of soluble salts

The results obtained from the elemental and molecular spectroscopic analyses suggest that all the building materials used for the Villa Belza construction are affected by the

crystallization of mainly sulfate and chloride salts. To confirm the magnitude of this impact, soluble salts were extracted and quantified to determine their specific nature. The concentrations of the anions and cations obtained after the soluble salts test are presented in Figure 5 (see also Table S1 in Supplementary Material). The results are expressed as the average concentration of each ion together with the relative standard deviation (at 95% confidence interval) calculated from three sample portions (subsamples) for each sample.

Regarding the quantified ions, the twenty-three building material samples showed the presence of Li^+ and NH_4^+ at low concentrations. Lithium is one of the most common cations present in marine aerosol **(Weller et al., 2008)**. Although the presence of ammonium in sea spray as ammonium nitrate (NH_4NO_3) and ammonium sulfate ($(NH_4)_2SO_4$) **(Guth et al., 2018; Park et al., 2018)** is widely known, the concentrations determined in all the samples are quite low (average of 28 mg/kg approximately). This could be related with the high solubility of ammonia. The concentration of NH_4^+ in other works related with buildings close to the sea at the Atlantic coast was similarly low (under limit of detection or even non-detected) **(García-Florentino et al., 2016)**.

Regarding alkali and alkaline earth cations, the concentrations in general terms are higher for Mg^{2+} than for K^+ (506 vs 485 mg/kg respectively). On the one hand, the samples that contain more than 600 mg/kg of K^+ are S3, S4, S20 and S23. Moreover, these three samples have a similar calcite proportion (around 50 %). Calcite is a very soluble compound, in the continuous contact with the H_2CO_3 aerosol, which can react after solubilization with other anions and cations coming from the sea spray giving rise to different K^+ compounds **(Morillas et al., 2013)**. On the other hand, as can be seen in the bar chart of Figure 5, the samples that show the highest concentrations of Mg^{2+} are S9, S12, S13, S14, S17 and S19 samples. For the unique only sandstone sample (S9) analyzed in this work, 8% (wt %) of dolomite was detected (see Table 1), thus the high Mg^{2+} concentration could be related with the presence of this carbonate. On the contrary, in the rest of the samples where high concentrations of Mg^{2+} were determined, dolomite was not identified. The high presence of this cation could be related with the presence of salts including this alkaline earth cation such as epsomite ($MgSO_4 \cdot 7H_2O$). Although this compound was not observed, neither by means of XRD nor by means of Raman spectroscopy, its presence cannot be discarded because this decay compound is very common to find in buildings close to the sea **(López-Arce et al., 2009)**.

The highest concentration of cations were registered for $Ca^{2+}$and Na^{+}. Calcium was one of the most concentrated elements (average concentration around 14236 ± 4790 mg/kg). This matches with the XRD and Raman analyses where calcite and gypsum were detected and this element is thus related with the presence of these compounds. In the samples S4 (rendering mortar) and S15 (joint mortar), where the highest concentration of Ca^{2+} was observed, decay compounds such as portlandite and ettringite were detected. The presence of Na^{+} (average concentration of 5068 ± 3102 mg/kg) in all the samples is closely related with the halite (NaCl) salts crystallizations detected in the samples **(Cardell et al., 2003)**. The concentration of Na^{+} is the highest in samples S3, S4 and S23 (11960, 10890 and 11330 mg/kg for S3, S4 and S23 respectively). This observation matches with the XRD results (see Table 1), where besides that these three samples have a similar calcite proportion (around 50 %), they have the highest proportion of halite (2%). In marine environments, for approximately every 5000 mg/kg of Na^{+} concentration, the construction material can be lost 1% (wt %) (due to spalling) and form halite in marine environments induced by marine aerosol.

Finally, the highest concentrations of anions are those of Cl^{-} and SO_4^{2-}, with average concentrations of 9254 ± 7002 and 10926 ± 8328 mg/kg respectively. Samples S3, S4 and S23 show the highest Cl^{-} and Na^{+} concentration. This observation corroborates the findings presented above in which the halite was detected clearly in the three cases. Moreover, samples S1, S2, S10, S11, S12, S13, S15 and S20 hold the higher SO_4^{2-} concentrations. According to Table 1, all of these sulfate concentrations are related with the presence of gypsum ($CaSO_4 \cdot 2H_2O$) in these samples except for the case of S15 for which the sulfate is linked to the presence of ettringite ($Ca_6Al_2(SO_4)_3(OH)_{12} \cdot 26H_2O$).

4. Conclusions

The multianalytical methodology based on the use of XRD and Raman spectroscopy for molecular analyses and μ-ED-XRF for elemental analyses, together with soluble salts quantification by means of ion chromatography allowed to define the nature and concentration of the salts which affect the conservation state of the building materials (limestone, sandstone, rendering and joint mortars) used in a construction next to the sea, the Villa Belza building.

Thanks to XRD and Raman spectroscopy, it was possible to identify different kind of sulfate crystallizations in building materials, whose concentration was set around 0.08-3

% depending the considered building material. The identification of gypsum, dehydrated and hemihydrated calcium sulfates (anhydrite and basanite) suggests that dehydration/hydration cycles are taking place in the materials, which promote a volume/size change in the salt crystallized in their pores, which can be responsible for crack formations and fissures in the building material.

Apart from sulfates, chlorines were also detected by XRD. Considering the limit of detection of the technique (around 1% (wt %), it becomes mandatory to use additional techniques to detect its presence. To perform a non-invasive study, μ-EDXRF imaging will be a good alternative, which allows to perform a screening of the samples to detect the presence of chlorine salts crystallizations. In the Villa Belza building materials, Na and Cl maps showed a coincident distribution, confirming the presence of halite in the samples. Thanks to the soluble salts test, it was possible to asses that the concentration of chlorides was between 0.1 and 3 %.

According to the extracted results, it can be affirm that this methodology can be integrated as a routine tool to extract conclusions related to the conservation state of building materials. In this case, that the building materials of Villa Belza are notoriously affected by the influence of marine aerosol, being the main cause of salts crystallizations. Building materials affected by salts can be desalinated following different procedures and methodologies (e.g., chemical and mechanical methods, use of slaughter mortars, immersion baths, electrochemical methods, etc.). However, the constant input of salts coming from marine aerosol will promote subsequent crystallization in the materials. In this sense, for future restorations of the construction, if the materials will be replaced, appropriate materials resistant to this influence should be selected. Therefore, this methodology capable of determining the original composition of the affected building material and the nature and content of the newly formed salts can be useful for civil engineers, architects, restorers and other scientist that aim to preserve building materials of constructions erected not only in a marine environment, but also in other locations affected by different environmental stressors.

Acknowledgements

The authors gratefully acknowledge the financial support from the Communauté d'agglomération Pau Béarn Pyrénées, from the ED211 doctoral school and from the project IT-742-13 for Consolidated Research Groups, funded by the Basque Government. The authors are thankful to the TMH restoration company who granted the access to the Villa Belza during its restoration. The authors also thank Professor Isabel Salcedo (Department of Plant Biology and Ecology, University of the Basque Country). D. Gregoire is fellow of the Institut Universitaire de France.

References

Bao, H., Niggemann, J., Luo, L., Dittmar, T., Kao, S-J., Molecular composition and origin of water-soluble organic matter in marine aerosols in the Pacific off China. Atmos. Environ. 191 (2018) 27-35.

Broomfield, J.P., Corrosion of Steel in Concrete: Understanding, Investigation and Repair, Publisher: CRC Press, ed. Taylor & Francis (London, UK), 2006.

Calparsoro, E., Maguregui, M., Giakoumaki, A., Morillas, H., Madariaga, J.M., Evaluation of black crust formation and soiling process on historical buildings from the Bilbao metropolitan area (north of Spain) using SEM-EDS and Raman microscopy. Environ. Sci. Pollut. Res. 24 (2017) 9468-9480.

Cardell, C., Delalieux, F., Roumpopoulos, K., Moropoulou, A., Auger, F., Van Grieken, R., Salt-induced decay in calcareous stone monuments and buildings in a marine environment in SW France, Construct. Build. Mater. 17(3) (2003) 165-179.

Ceburnis, D., Rinaldi, M., Ovadnevaite, J., Martucci, G., Giulianelli, L., O'Dowd, C. D., Marine submicron aerosol gradients, sources and sinks. Atmos. Chem. Phys. 16(19) (2016) 12425-12439.

Celik, M. Y., Aygun, A., The effect of salt crystallization on degradation of volcanic building stones by sodium sulfates and sodium chlorides, B. Eng. Geol. Environ. (2018) Ahead of Print.

Chunran, W., Shicong K, Effects of high-calcium sepiolite on the rheological behaviour and mechanical strength of cement pastes and mortars, Construct. Build. Mater. 196 (2019) 105-114.

483 Cultrone, G., Sebastian, E., Laboratory simulation showing the influence of salt
484 efflorescence on the weathering of composite building materials, Environ. Geol.
485 56(3-4) (2008) 729-740.

486 Derluyn, H., Griffa, M., Mannes, D., Jerjen, I., Dewanckele, J., Vontobel, P., Sheppard,
487 A., Derome, D., Cnudde, V., Lehmann, E., Carmeliet, J., Characterizing saline
488 uptake and salt distributions in porous limestone with neutron radiography and
489 X-ray micro-tomography, J. Build. Phys. 36 (2013) 353-374.

490 Derluyn, H., Dewanckele, J., Boone, M. N., Cnudde, V., Derome, D., Carmeliet, J.,
491 Crystallization of hydrated and anhydrous salts in porous limestone resolved by
492 synchrotron x-ray microtomography, Nucl. Instrum. Meth. B 324 (2014) 102-
493 112

494 Derluyn, H., Vontobel, P., Mannes, D., Derome, D., Lehmann, E., Carmeliet, J., Saline
495 Water Evaporation and Crystallization-Induced Deformations in Building Stone:
496 Insights from High-Resolution Neutron Radiography, Transport Porous Med.
497 128(3) (2019) 895-913.

498 Elsen, J., Microscopy of historic mortars—a review, Cem. Concr. Res. 36 (2006) 1416-
499 1424.

500 Espinosa, R.M., Franke, L., Deckelmann, G., Model for the mechanical stress due to the
501 salt crystallization in porous materials, Construct. Build. Mater. 22 (2008a)
502 1350-1367.

503 Espinosa, R.M., Franke, L., Deckelmann, G., Phase changes of salts in porous
504 materials: Crystallization, hydration and deliquescence, Construct. Build. Mater.
505 22 (2008b) 1758-1773.

506 García-Florentino, C., Maguregui, M., Morillas, H., Balziskueta, U., Azcarate, A.,
507 Arana, G., Madariaga, J.M., Portable and Raman imaging usefulness to detect
508 decaying on mortars from Punta Begoña Galleries (Getxo, North of Spain), J.
509 Raman Spectrosc. 47 (2016) 1458-1466

510 Gómez-Heras, M., Fort, R., Patterns of halite (NaCl) crystallisation in building stone
511 conditioned by laboratory heating regimes, Environ. Geol. 52(2) (2007) 259-
512 267.

513 Granneman, S. J. C., Lubelli, B., van Hees, R. P. J., Effect of mixed in crystallization
514 modifiers on the resistance of lime mortar against NaCl and Na_2SO_4
515 crystallization. Construct. Build. Mater. 194 (2019) 62-70.

516 Guth, J., Marecal, V., Josse, B., Arteta, J., Hamer, P., Primary aerosol and secondary
517 inorganic aerosol budget over the Mediterranean Basin during 2012 and 2013,
518 Atmos. Chem. Phys., 18 (2018) 4911-4934.

519 Hansen, H.C.B., Taylor, R.M., Formation of synthetic analogues of double metal-
520 hidroxy carbonate minerals under controlled pH conditions: I. The synthesis of
521 Pyroaurite and Reevesite, Clay Miner. 25 (1990) 161-179

522 Kamh, G. M. E., Koltuk, S., Ismael, H., Refinement of categorization and scaling of
523 weathering-related damage to natural stone: case study on oolitic limestone from
524 El-Shatbi Tombs (Egypt). B. Eng. Geol. Environ. 76(1) (2017) 39-57.

525 Lopez-Arce, P., Doehne, E., Greenshields, J., Benavente D., Young, D., Treatment of
526 rising damp and salt decay: the historic masonry buildings of Adelaide, South
527 Australia, Mater. Struct. 42(6) (2009) 827-848.

528 Mendonça Filho, F.F., Morillas, H., Derluyn, H., Maguregui, M., Gregoire, D., In-situ
529 versus laboratory characterization of historical site in marine environment using
530 X-ray fluorescence and Raman spectroscopy, Microchem. J. 147 (2019) 905-
531 913.

532 Miyazaki, Y., Yamashita, Y., Kawana, K., Tachibana, E., Kagami, S., Mochida, M.,
533 Suzuki, K., Nishioka, J., Chemical transfer of dissolved organic matter from
534 surface seawater to sea spray water-soluble organic aerosol in the marine
535 atmosphere, Scientific Reports 8(1) (2018) 1-10.

536 Molina, E., Cultrone, G., Sebastián, E., Alonso, F. J., Carrizo, L., Gisbert, J., Buj, O.,
537 The pore system of sedimentary rocks as a key factor in the durability of
538 building materials, Eng. Geol. 118 (2011) 110-121.

539 Morillas, H., Maguregui, M., Gomez-Laserna, O., Trebolazabala, J., Madariaga, J.M.,
540 Could marine aerosol contribute to deteriorate building materials from interior
541 areas of lighthouses? An answer from the analytical chemistry point of view, J.
542 Raman Spectrosc. 44 (2013) 1700-1710.

543 Morillas, H., Maguregui, M., Trebolazabala, J., Madariaga, J.M., Nature and origin of
544 white efflorescence on bricks, artificial stones, and joint mortars of modern
545 houses evaluated by portable Raman spectroscopy and laboratory analyses,
546 Spectrochim. Acta A 136 (2015) 1195-1203.

547 Morillas, H., Maguregui, M., García-Florentino, C., Marcaida, I., Madariaga, J.M.,
548 Study of particulate matter from Primary/Secondary Marine Aerosol and
549 anthropogenic sources collected by a self-made passive sampler for the
550 evaluation of the dry deposition impact on Built Heritage, Sci. Total Environ.
551 550 (2016a) 285-296.

552 Morillas, H., García-Galán, J., Maguregui, M., Marcaida, I., García-Florentino, C.,
553 Carrero, J.A., Madariaga, J.M., Assessment of marine and urban-industrial
554 environments influence on built heritage sandstone using X-ray fluorescence
555 spectroscopy and complementary techniques, Spectrochim. Acta B 123 (2016b)
556 76–88.

557 Morillas, H., Marcaida, I., García-Florentino, C., Maguregui, M., Arana, G., Madariaga,
558 J.M, Micro-Raman and SEM-EDS analyses to evaluate the nature of salt clusters
559 present in secondary marine aerosol, Sci. Total. Environ. 615 (2018a) 691-697.

560 Morillas, H., Garcia-Florentino, C., Marcaida, I., Maguregui, M., Arana, G., Silva, L. F.
561 O., Madariaga, J. M., In-situ analytical study of bricks exposed to marine
562 environment using hand-held X-ray fluorescence spectrometry and related
563 laboratory techniques, Spectrochim. Acta B 146 (2018b) 28-35.

564 O'Dowd, C.D., de Leeuw, G., Marine aerosol production: a review of the current
565 knowledge. Phil. Trans. R. Soc. A 365 (2007) 1753-1774.

566 Onasch, T.B., McGraw, R., Imre, D., Temperature-Dependent Heterogeneous
567 Efflorescence of Mixed Ammonium Sulfate/Calcium Carbonate Particles, J.
568 Phys. Chem. A 104 (2000) 10797-10806.

569 Park, M., Joo, H.S., Lee, K., Jang, M., Kim, S.D., Kim, I., Borlaza, L.J.S., Lim, H.,
570 Shin, H., Chung, K.H., Choi, Y-H., Park, S.G., Bae, M-S., Lee, J., Song, H.,
571 Park, K., Differential toxicities of fine particulate matters from various sources,
572 Scientific Reports 8(1) (2018) 1-11.

Prieto-Taboada, N., Gómez-Laserna, O., Martínez-Arkarazo, I., Olazabal, M.A., Madariaga, J.M., Optimizations of two methods based on ultrasound energy as alternative to European standards from soluble salts extraction from building materials, J. Ultrasound Sonochem. 19(6) (2012) 1260-1265.

Raneri, S., Cnudde, V., De Kock, T., Derluyn, H., Barone, G., Mazzoleni, P., X-ray computed micro-tomography to study the porous structure and degradation processes of a building stone from Sabucina (Sicily), Eur. J. Mineral. 27(3) (2015) 279-288.

Rosina, E., Sansonetti, A., Erba, S., Focus on soluble salts transport phenomena: The study cases of Leonardo mural paintings at Sala delle Asse (Milan), Construct. Build. Mater. 136 (2017) 643-652.

Ruedrich, J., Seidel, M., Rothert, E., Siegesmund, S., Length changes of sandstones caused by salt crystallization, Geol. Soc. Spec. Publ. 271(1) (2007) 199-209.

Shalygin, S., Kavulic, K.J., Pietrasiak, N., Bohunicka, M., Vaccarino, M.A., Chesarino, N.M., Johansen, J.R., Neotypification of Pleurocapsa fuliginosa and epitypification of P. minor (Pleurocapsales): resolving a polyphyletic cyanobacterial genus, Phytotaxa 392(4) (2019) 245-263.

Thiebaut, Y., Multon, S., Sellier, A., Lacarrière, L., Boutillon, L., Belili, D., Linger, L., Cussigh, F., Hadji, S., Effects of stress on concrete expansion due to delayed ettringite formation, Construct. Build. Mater. 183 (2018) 626-641.

Vallet, J. M., Gosselin, C., Bromblet, P., Rolland, O., Verges-Belmin, V., Kloppmann, W., Origin of salts in stone monument degradation using sulphur and oxygen isotopes: First results of the Bourges cathedral (France). J. Geochem. Explor. 88(1-3) (2006) 358-362.

Weller, R., Woeltjen, J., Piel, C., Resenberg, R., Wagenbach, D., Koenig-Langlo, G., Kriews, M., Seasonal variability of crustal and marine trace elements in the aerosol at Neumayer station, Antarctica, Tellus B 60B(5) (2008) 742-752.

Xiao, H-W., Xiao, H-Y., Luo, L., Zhang, Z-Y., Huang, Q-W., Sun, Q-B., Zeng, Z-Q., Stable carbon and nitrogen isotope compositions of bulk aerosol samples over the South China Sea. Atmos. Environ. 193 (2018) 1-10.

603 Yang, J., Wang, F., Influence of assumed absorption capacity of superabsorbent
604 polymers on the microstructure and performance of cement mortars, Construct.
605 Build. Mater. 204 (2019) 468-478.

606 Zezza, F., Macrì, F., Marine aerosol and stone decay, Sci. Total Environ. 167(1-3)
607 (1995) 123-143.

608 Zhang, Q-N., Zhang, Y., Cai, C., Guo, Y-C., Reid, J. P., Zhang, Y-H, In Situ
609 Observation on the Dynamic Process of Evaporation and Crystallization of
610 Sodium Nitrate Droplets on a ZnSe Substrate by FTIR-ATR, J. Phys. Chem. A
611 118(15) (2014) 2728-2737.

612 Zhou, X., Liu, D., Bu, H., Deng, L., Liu, H., Yuan, P., Du, P., Song, H., XRD-based
613 quantitative analysis of clay minerals using reference intensity ratios, mineral
614 intensity factors, Rietveld, and full pattern summation methods: a critical review.
615 Solid Earth Sci. 3 (2018) 16-29.

616

617 ## FIGURE CAPTIONS

618 **Figure 1.** Location, type of material and sampling of the 23 samples from Villa Belza
619 building (Biarritz, France).

620 **Figure 2.** XRD of building materials in Villa Belza of **A)** S4 (rendering mortar) with
621 the presence of calcite ($CaCO_3$), quartz (SiO_2), halite (NaCl) and portlandite ($Ca(OH)_2$)
622 and **B)** S15 (joint mortar) with the presence of quartz (SiO_2), calcite ($CaCO_3$), ettringite
623 ($Ca_6Al_2(SO_4)_3(OH)_{12}.26H_2O$) and pyroaurite ($Mg_6Fe_2(CO_3)(OH)_{16}.4H_2O$).

624 **Figure 3.** Raman spectra of S1, S2, S9, S10, S11, S12, S13, S14 and S20, indicating the
625 presence of **A)** gypsum ($CaSO_4 \cdot 2H_2O$); **B)** basanite ($CaSO_4 \cdot ½H_2O$) and **C)** anhydrite
626 ($CaSO_4$).

627 **Figure 4.** μ-ED-XRF imaging of the S15 sample from Villa Belza (Biarritz, France)
628 showing the elemental distribution maps of some of the detected elements. (For
629 interpretation of the references to color in this figure, the reader is referred to the web
630 version of this article.)

631 **Figure 5.** Bar charts showing cations and anions concentrations (mg/kg units) on each
632 Villa Belza sample.

633

634
635
636
637
638
639

Table 1
Click here to download Table: Table 1.docx

Table 1. Semi-quantitative information of mineralogical phases detected by XRD in the analyzed samples from Villa Belza (Biarritz, France).

Samples	Type of Material	Calcite ($CaCO_3$)	Gypsum ($CaSO_4 \cdot 2H_20$)	Halite (NaCl)	Quartz (SiO_2)	Mica ($AC_2{}_{-3}T_4O_{10}X_2$)	Dolomite ($CaMg(CO_3)_2$)	Microcline ($KAlSi_3O_8$)	Kaolinite ($Al_2Si_2O_5(OH)_4$)	Portlandite ($Ca(OH)_2$)	Ettringite $Ca_6Al_2(SO_4)_3(OH)_{12}.26H_2O$	Pyroaurite $Mg_6Fe_2(CO_3)(OH)_{16}.4H_2O$
S1	Limestone	96 %	4 %	< 1 %	-	-	-	-	-	-	-	-
S2	Limestone	93 %	3 %	1 %	3 %	-	-	-	-	-	-	-
S3	Rendering mortar	50 %	-	2 %	48 %	-	-	-	-	-	-	-
S4	Rendering mortar	41 %	-	2 %	54 %	-	-	-	-	2 %	-	-
S5	Rendering mortar	39 %	-	< 1 %	61 %	-	-	-	-	-	-	-
S6	Rendering mortar	51 %	-	< 1 %	49 %	-	-	-	-	-	-	-
S7	Limestone	92 %	-	-	8 %	< 1 %	-	-	< 1 %	-	-	-
S8	Rendering mortar	12%	-	-	88 %	-	-	-	-	-	-	-
S9	Sandstone	55 %	2 %	1 %	34 %	-	8 %	-	-	-	-	-
S10	Limestone	96 %	4 %	-		-	-	-	-	-	-	-
S11	Limestone	95 %	5 %	-		-	-	-	-	-	-	-
S12	Rendering mortar	15 %	3 %	-	82 %	-	-	-	-	-	-	-
S13	Sandstone	2 %	2 %	1 %	95 %	-	-	-	-	-	-	-
S14	Sandstone	14 %	4 %	-	82 %	-	-	-	-	-	-	-
S15	Joint mortar	28 %	-	-	67 %	-	-	-	-	-	4 %	1 %
S16	Sandstone	15 %	-	-	75 %	-	-	10 %	-	-	-	-
S17	Joint mortar	28 %	-	-	70 %	-	2 %	-	-	-	-	-
S18	Cement	17 %	-	1 %	82 %	-	-	-	-	-	-	-
S19	Rendering mortar	16 %	-	< 1 %	84 %	-	-	-	-	-	-	-
S20	Sandstone	12 %	7 %	1 %	80 %	-	-	-	-	-	-	-
S21	Rendering mortar	14 %	-	< 1 %	86 %	-	-	-	-	-	-	-
S22	Limestone	75 %	-	< 1 %	24 %	-	-	-	-	-	-	-
S23	Rendering mortar	49 %	-	2 %	49 %	-	-	-	-	-	-	-

Figure 1

Click here to download high resolution image

Figure 2

Click here to download high resolution image

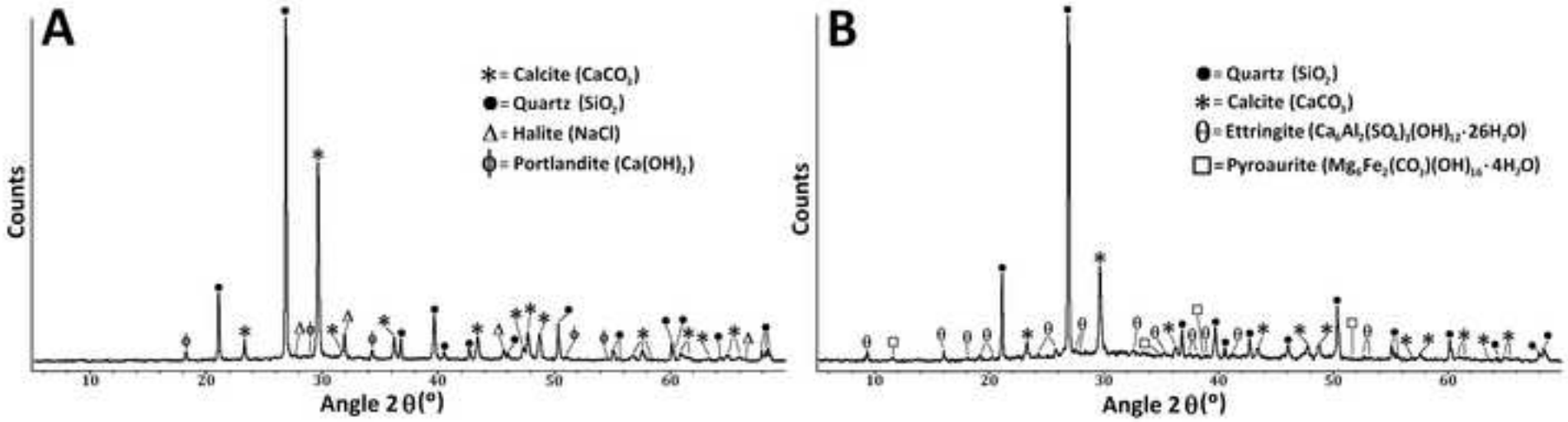

Figure 3

Click here to download high resolution image

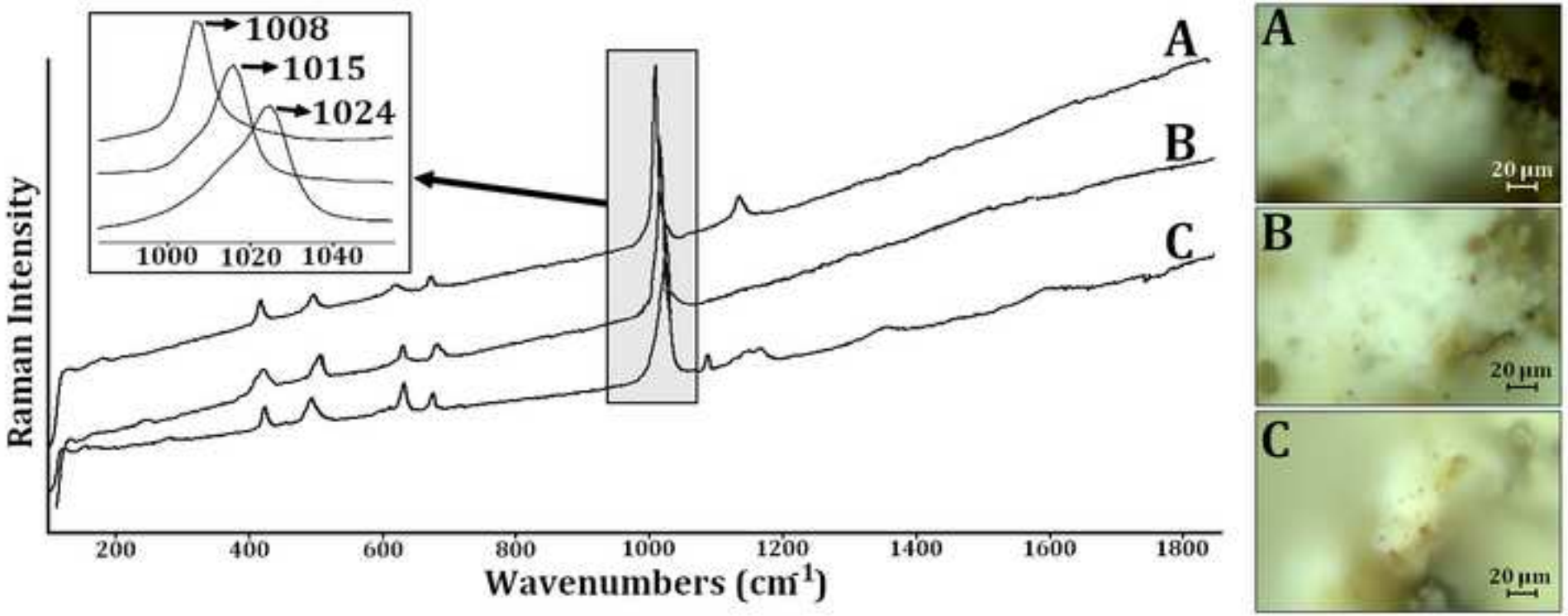

Figure 4

Click here to download high resolution image

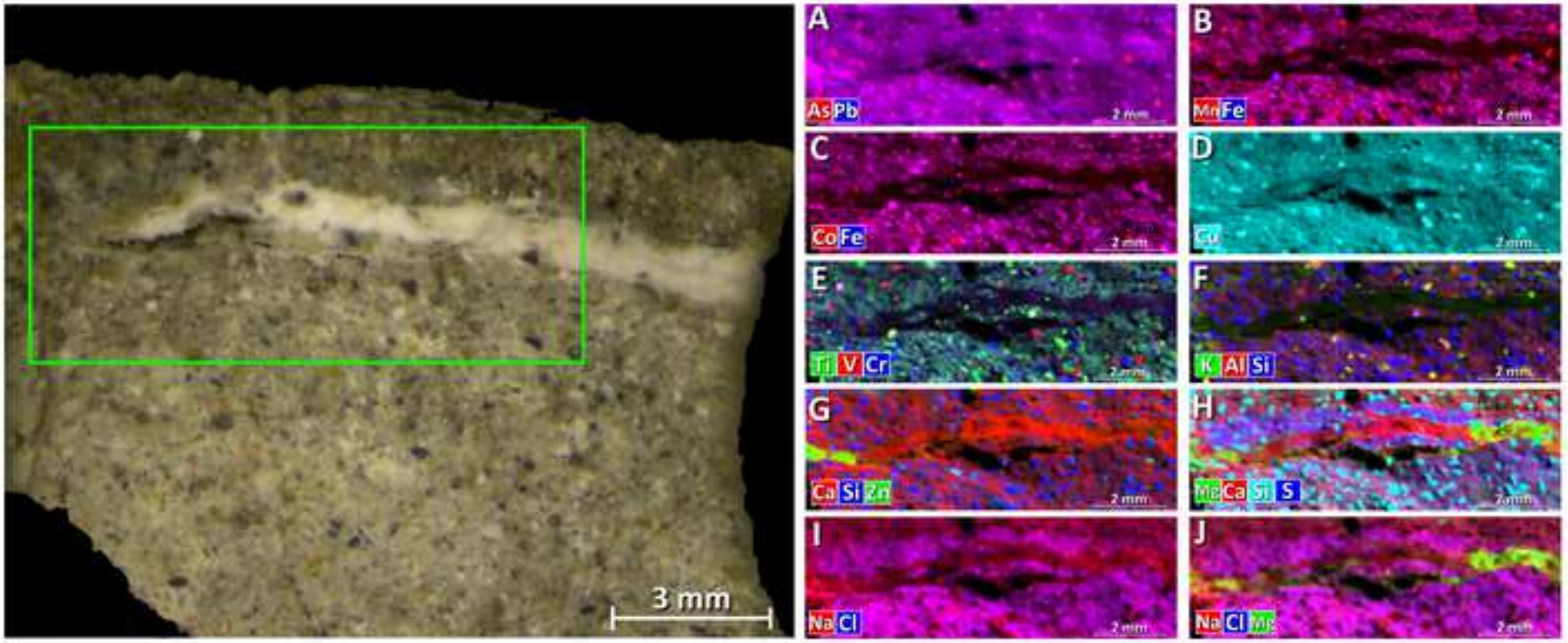

Figure 5

Click here to download high resolution image